Renewable Energy 108 (2017) 425–437

Contents lists available at ScienceDirect

Renewable Energy

journal homepage: www.elsevier.com/locate/renene

Performance comparison of the floating and fully submerged quasi-point absorber wave energy converters

N.Y. Sergiienko*, B.S. Cazzolato, B. Ding, P. Hardy, M. Arjomandi

The University of Adelaide, School of Mechanical Engineering, Adelaide, Australia

ARTICLE INFO

Article history:
Received 2 August 2016
Received in revised form
6 January 2017
Accepted 1 March 2017
Available online 3 March 2017

Keywords:
Wave energy converter
Submerged point absorber
Floating point absorber
Power generation

ABSTRACT

Axisymmetric point absorbers are mostly designed as floating buoys that extract power from heave motion. Power absorption limits of such wave energy converters (WECs) are governed by the displaced volume of the buoy and its ability to radiate waves. In the case of fully submerged WECs, the power performance becomes a function of additional variables including the proximity to the mean surface level of the water, body shape and the maximum stroke length of the power take-off system. Placing the body below the water surface increases its survivability in storm conditions but changes the hydrodynamic properties of the WEC including maximum absorbed power. This paper investigates the differences between floating and fully submerged point absorber converters from the number of perspectives including energy extraction, bandwidth, and optimal size for a particular wave climate. The results show that when compared with floating converters, fully submerged buoys: (i) generally absorb less power at longer wavelengths, (ii) have narrower bandwidth, (iii) cannot be replaced by smaller units of the same total volume without a significant loss of power, and (iv) have a significant advantage as they can effectively utilise several modes of motion (e.g. surge and heave) in order to increase power generation.

1. Introduction

Intensive research on extraction energy from ocean waves started in the 1970s [1]. Initially, attention was paid to the terminator-type converters which were studied as two-dimensional devices with an infinitely long body extension perpendicular to the wave front (e.g. Salter's duck [2]). However, due to the sensitivity of such prototypes to the direction of wave propagation, researchers focussed on the concept of a point-absorbing wave energy converter (WEC) [3] whose performance does not depend on the angle of wave incidence. Thereafter, point absorbers (PA) have become one of the most studied WECs, making up a large part of existing full-scale prototypes.

Generally, PAs are designed to operate on or just below the water surface, extracting wave power from the heaving motion. As opposed to submerged buoys, floating converters require less installation and maintenance work under water. However, there could be several very important reasons to keep the WEC fully submerged (see Fig. 1):

(i) to increase the survivability of the converter during storms with large wave conditions;
(ii) when there is an unconditional requirement from the public authorities to minimise visual impact of the wave power generator, e.g. the buoy must not be visible from the shore.

Based on the fundamental equations of maximum power absorption for axisymmetric bodies, floating and submerged WECs are able to extract the same amount of wave power provided unconstrained motion amplitudes [3,4]. Thus, under this condition the maximum capture width of the oscillating body does not depend on its size, shape or submergence depth, but is governed by the mode of motion [5,6]. According to these findings, the body that moves in surge and heave simultaneously can absorb three times more power than a heaving buoy.

In practice, WEC motion should be constrained during large waves, hence power absorption becomes dependent on the maximum allowed oscillation amplitude and the wave excitation force exerted on the converter [7,8]. As the latter is determined by the shape, size and submergence depth of the WEC, it becomes apparent that identical fully submerged and floating buoys cannot capture the same amount of wave energy. It has been observed [1] that submerged converters are poorer wave absorbers as compared

* Corresponding author.
E-mail address: nataliia.sergiienko@adelaide.edu.au (N.Y. Sergiienko).

http://dx.doi.org/10.1016/j.renene.2017.03.002
0960-1481/

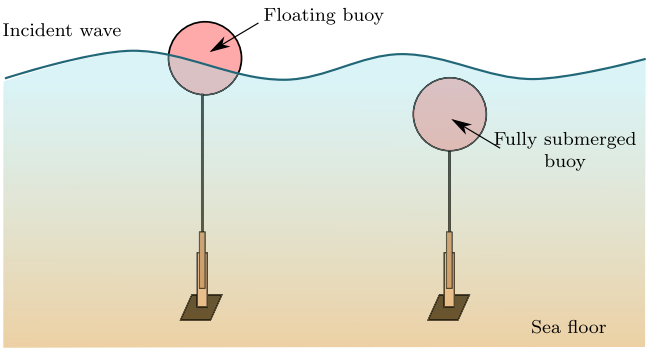

Fig. 1. Schematic representation of the floating and fully submerged WECs that extract energy from oscillations in heave.

to the floating heaving buoys because their upper and lower portions of the swept volume have different polarities during the oscillatory motion. In addition, floating and fully submerged WECs have distinctive low-frequency limits of the heave excitation forces. As the wave frequency tends to zero, the amplitude of the heave force on the floating body is limited by the hydrostatic stiffness coefficient, whereas for the fully submerged converter the excitation force approaches zero due to the diminishing water plane area [5]. Subsequently, based on these findings and also taking into account the swept volume of the body, Budal [9] was able to formulate power absorption bounds for floating WECs that oscillate in heave. This approach has been extended to the fully submerged buoys where the expressions of the power limits for several basic geometries are derived [10]. However, it may be concluded that in the case of point-absorbing WECs, the main research focus has been drawn to the floating buoys, while some features of submerged converters still remain unclear or have not been sufficiently explored.

The current paper provides a systematic comparison between floating and submerged PAs by generalising existing knowledge and providing an in-depth analysis. All results are based on the linear wave theory assuming regular and irregular wave conditions and infinite water depth. Background information and power absorption limits of heaving PA systems are presented in Section 2. Key features of different control strategies are discussed in Section 3, followed by the methods of selecting the correct size of the converter in Sections 4–5. Finally, the possibility of extracting power from additional modes of motion is reported in Section 6.

2. Power limits for regular waves

A body placed in water captures wave energy only when it moves in an oscillatory manner and radiates waves in order to counteract the incident wave front. Thus, the maximum amount of power that can be removed from waves is defined by the radiating ability of the body. This limit has been derived in Refs. [3,4,11] and differs for motion modes. A well known equation characterising the maximum absorbed power by an axisymmetric body in monochromatic waves is [5]:

$$P_{\max} = \alpha \frac{J}{k}, \tag{1}$$

where $J = \rho g^2 D(kh) A^2/(4\omega)$ is the wave-energy transport per unit frontage of the incident wave, α is a coefficient that depends on the motion oscillation mode ($\alpha = 1$ for heave, $\alpha = 2$ for surge or pitch, and $\alpha = 3$ when the body oscillates in heave, surge and pitch simultaneously), k is the wavenumber, A is the wave amplitude, ρ is water density, ω is the wave frequency and $D(kh)$ is the depth function which is equal to 1 for deep water.

Maximum power in Equation (1) is obtained when the body velocity is [5]:

$$\widehat{u}_{j,opt}(\omega) = \frac{\widehat{F}_{j,exc}(\omega)}{2B_{jj}(\omega)}, \tag{2}$$

where $\widehat{F}_{j,exc}$ is the wave excitation force on the body in mode j, and B_{jj} is the radiation damping coefficient in mode j. However, the amount of power in waves with long period is very high and in order to absorb the absolute maximum, the body should move with large amplitudes at high velocities which is not achievable in practice. Thus, if $|\widehat{u}_j| < |\widehat{u}_{j,opt}|$, the amount of radiated power (P_r) will be much smaller than the excitation power (P_e) and the absorbed power will be limited by the latter:

$$P = P_e - P_r \le \frac{1}{2}\left|\widehat{F}_{j,exc}\widehat{u}_j\right|. \tag{3}$$

According to Equation (3), Budal (as cited in Ref. [1]) showed that the power extraction at low frequencies is limited by the swept volume of the body, which is a collective term for the body physical volume and the maximum motion amplitude. Thus, for the floating body, the motion amplitude in heave is constrained by its vertical dimension, such that $|\widehat{s}_3| < V/(2S_w)$, where V is the body volume, S_w is the water-plane area of the body, and the subscript $j = 3$ corresponds to the heave motion. Therefore, the maximum velocity in heave cannot be larger than $|\widehat{u}_3| < \omega V/(2S_w)$. Furthermore, the heave excitation force is bounded by the integrated pressure force over the water-plane area of the body, which is $\left|\widehat{F}_{3,exc}\right| < \rho g S_w A$. As a result, the power absorption of the floating heaving buoy has two boundaries:

(i) a high-frequency limit P_A defined by the body's ability to radiate waves (from Equation (1) assuming deep water conditions $\omega^2 = kg$):

$$P_A = \frac{J}{k} = \frac{\rho g^2 A^2}{4\omega k} = \frac{\rho g^3 \left(\frac{H}{2}\right)^2}{4\omega^3} = c_\infty T^3 H^2, \tag{4}$$

where $c_\infty = \rho(g/\pi)^3/128$, $H = 2A$ is the wave height, $T = 2\pi/\omega$ is the wave period;

(ii) a low-frequency limit P_B defined by the maximum swept volume of the body, which applies when the velocity of the converter is smaller than the optimal value due to physical constraints:

$$P_{B,f} = \frac{1}{2}\left|\widehat{F}_{3,exc}\widehat{u}_3\right| = \frac{\rho g \omega V A}{4} = \frac{c_0 V H}{T}, \tag{5}$$

where $c_0 = (\pi/4)\rho g$ and the subscript f corresponds to the floating case.

These boundaries have been derived for floating bodies that move in heave only regardless of shape. In general, the P_A-limit depends only on the mode of motion and has the same expression for submerged and floating bodies. With regard to the P_B curve, the power absorption limit of the fully submerged converter is strongly dependent on shape and should be derived for each case under consideration independently. Thus, for a spherical body with its centre placed d_s below the water surface, the P_B-limit can be expressed as [10]:

$$P_{B,s} = 4\pi^3 \rho e^{-kd_s} s_{3,\max} \frac{VH}{T^3}, \tag{6}$$

where the subscript s corresponds to the submerged case, and $s_{3,\max}$ is the maximum displacement of the sphere in heave.

To demonstrate the comparison between power limits for the floating and submerged WECs, three spherical bodies with different submergence depths have been chosen for the analysis as indicated in Fig. 2. All spheres have the same physical volume of 524 m^3 (radius is $a = 5$ m) and the motion amplitudes are constrained by $s_{3,\max} = 0.67a = 3.3$ m. Regular waves of height $H = 2$ m are considered. Hydrodynamic coefficients of all buoys have been obtained using WAMIT [12]. It should be noted that a sphere which is located in close proximity to the mean water level ($d_s = 6$ m) may breach the surface of the water during operation. In this case, the linear wave theory breaks down and thus provides only a rough approximation of the wave-body interaction. Also, in this work the wave parameters and dimensions of all WECs are selected such that the Keulegan-Carpenter (KC) number does not exceed π, thus avoiding excessive viscous losses in the system and ensuring that linear potential theory is considered valid [13].

The power extracted by the spherical WECs over the range of wave periods, assuming optimal reactive control, is displayed in Fig. 3. The most important difference between power absorption of floating and submerged heaving systems is that the latter has a faster decay rate at the low frequency range. Comparing Equations (5) and (6), it is obvious that $P_{B,f} = \mathcal{O}(T^{-1})$, while $P_{B,s} = \mathcal{O}(T^{-3})$, which leads to a decrease in power absorption at longer wavelengths. Moreover, due to the fact that the hydrodynamic pressure on the body surface decays exponentially with depth, the presence of $\exp(-kd_s)$ in Equation (6) shows a reduction of power for deeper submergences. Consequently, the sphere submerged to $2a = 10$ m extracts less power than that submerged to $1.2a = 6$ m. Whilst smaller excitation forces from low-frequency waves increase survivability of the system under storm conditions it comes at the expense of power generation.

The analysis will now be extended to cylindrical WECs with volume of 524 m^3, which is the same as for the spheres considered. The height to radius ratio of each cylinder is set to 1 leading to $h_c = a = 5.5$ m. Three different submergence depths are examined as shown in Fig. 4: one floating case, $d_s = 0$, and two submerged cases with $d_s = 0.5h_c + 1 = 0.68a = 3.75$ m and $d_s = h_c + 1 = 1.18a = 6.5$ m. The volume stroke in heave is set to be equal to the structural body volume leading to the motion constraints of $s_{3,\max} = 0.5h_c = 2.75$ m.

In contrast to the sphere, a vertical cylinder has a non-convex shape and if placed very close to the mean water level it will experience resonant motion of the fluid above its flat top surface [14]. This phenomenon causes a rapid change in the added mass, damping coefficients and excitation forces at the restricted

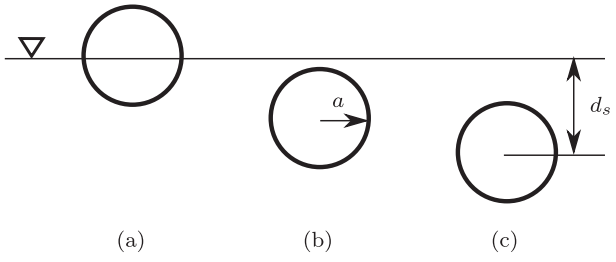

Fig. 2. Schematic representation of the floating and submerged spheres of radius $a = 5$ m: (a) $d_s = 0$, (b) $d_s = 1.2a = 6$ m and (c) $d_s = 2a = 10$ m.

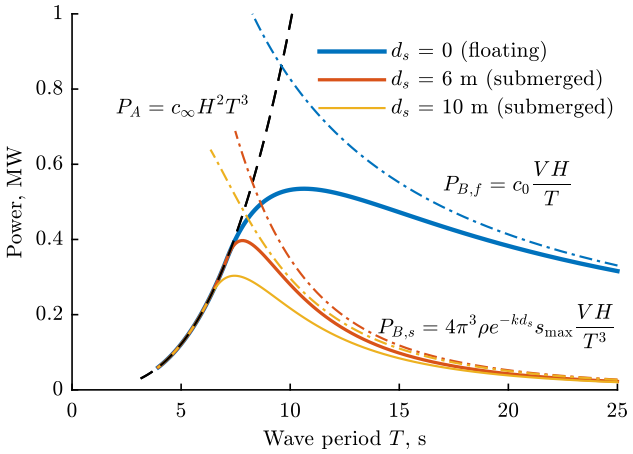

Fig. 3. Power absorbed by the floating and submerged spheres in regular waves vs. wave period. Sphere radius is $a = 5$ m, displacement in heave is constrained to $0.6a$, wave height is $H = 2$ m. The dashed curve corresponds to the P_A limit from Eq. (4), and three dash-dotted curves show the P_B bounds from Eqs. (5) and (6).

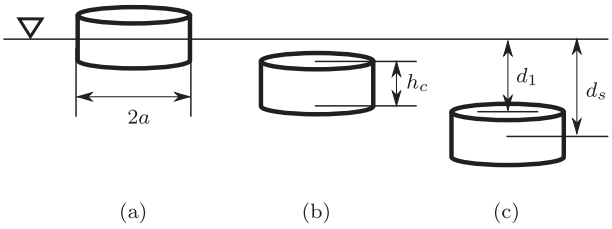

Fig. 4. Schematic representation of the floating and submerged truncated vertical cylinders, $h_c = a = 5.5$ m: (a) $d_s = 0$, (b) $d_s = 0.5h_c + 1 = 0.68a = 3.75$ m, (c) $d_s = h_c + 1 = 1.18a = 6.5$ m.

frequency range [15]. Therefore, the P_B-bound for the submerged cylinder has a more complicated expression than for the spherical case (for full derivation see Appendix A):

$$P_{B,s} = \frac{\pi^2 a \rho g H}{T} s_{3,\max} \left(\frac{2J_1(\kappa a)}{\kappa J_0(\kappa a) \cosh(\kappa d_1)} - a e^{-kd_2} \right), \tag{7}$$

where $d_2 = d_1 + h_c$, J_0 and J_1 are Bessel functions of the first kind of order 0 and 1 respectively, κ is the real solution of the dispersion equation $\omega^2 = g\kappa \tanh(\kappa d_1)$, which can be approximated by $\omega^2 = \kappa^2 g d_1$ using shallow water conditions for the water domain above the cylinder.

The variation of absorbed power over the range of wave periods for the three cylinders with different submergence depth is demonstrated in Fig. 5. Similar to the spherical case, the absorbed power of the submerged cylinders decays faster at longer wavelengths even though it cannot be clearly seen from Equation (7). Comparing power for spherical and cylindrical bodies, it is interesting to note that the performance of the cylinder placed close to the mean water level ($d_s = 3.75$ m) is better than that of the floating one within a particular range of wave periods ($7\text{ s} < T < 10\text{ s}$). However, if the cylinder is placed deep enough below the water surface, the power absorption is poorer for the submerged bodies across the entire frequency range as is shown for the $d_s = 6.5$ m case on Fig. 5.

3. Control performance

In this section, differences between floating and submerged

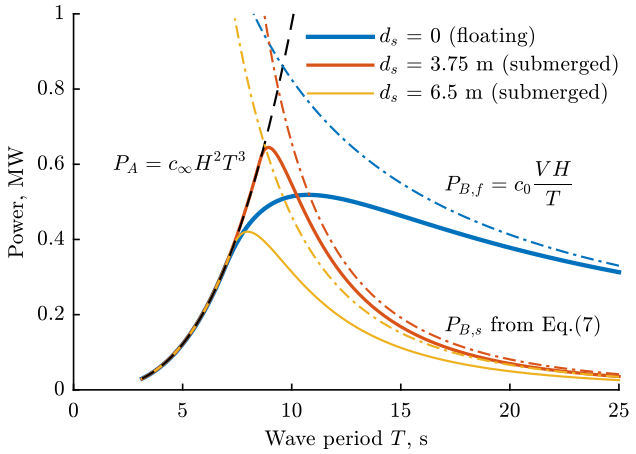

Fig. 5. Power absorbed by the floating and submerged truncated vertical cylinders in regular waves vs. wave period. Cylinder radius and height are $h_c = a = 5.5$ m, heave displacement is constrained to $0.5h_c$, wave height is $H = 2$ m. The dashed curve corresponds to the P_A limit from Eq. (4), and three dash-dotted curves show the P_B bounds from Eqs. (5) and (7).

converters are analysed from the control point view. Also, frequency domain analysis of power production is extended to the irregular wave conditions in the time domain.

3.1. Optimal reactive control

Power levels presented in Figs. 3 and 5 show the average absorbed power from reactively controlled WECs. In the frequency domain, the maximum power output is achieved by applying complex conjugate, or impedance matching, control [16]. The main idea that underlies this control strategy is to tune the resonance frequency of the system to the frequency of the incident wave by means of the load (control) force exerted on the buoy. However, despite the same control strategy applied to floating and submerged converters, there is a principal difference between their implementations which is governed by the presence (floating) or absence (fully submerged) of the hydrostatic restoring force.

The natural frequency of floating converters is defined by the hydrostatic stiffness that can bring a disturbed system to its equilibrium position. Thus, it can be calculated utilising a simple equation for the mass-spring-damper model:

$$\omega_0 = \sqrt{\frac{C}{m + A(\omega_0)}}, \tag{8}$$

where C is the hydrostatic stiffness, m is the mass of the buoy and $A(\omega_0)$ is the value of the buoy added mass at the natural frequency. However, in the case of fully submerged buoys the hydrostatic stiffness is absent and there is no restoring force that would keep the body submerged all the time (if body is lighter than water). Therefore, the natural frequency of submerged heaving WECs approaches 0 ($\omega_0 \to 0$) unless an external restoring force (spring) is applied to the system. This also relates to the floating and submerged bodies that move in surge as their natural frequency $\omega_0 \to 0$.

In addition to the natural frequency, the hydrostatic stiffness affects the optimal control force that is required for maximum power absorption. If the buoy is constrained to move in heave only, its motion in frequency domain can be described as [5]:

$$\widehat{Z}_i(\omega)\widehat{u}(\omega) = \widehat{F}_{exc}(\omega) + \widehat{F}_{pto}(\omega), \tag{9}$$

where $\widehat{F}_{pto}(\omega)$ is the control (power take-off) force applied to the buoy and the intrinsic mechanical impedance of the system $\widehat{Z}_i(\omega)$ has a form [5]:

$$\widehat{Z}_i(\omega) = B(\omega) + j\omega\left(m + A(\omega) - \frac{C}{\omega^2}\right). \tag{10}$$

In order to absorb maximum power, the control force $\widehat{F}_{pto}(\omega) = -\widehat{Z}_{pto}(\omega)\widehat{u}(\omega)$ should satisfy the optimal condition [5]:

$$\widehat{Z}_{pto}(\omega) = \widehat{Z}_i^*(\omega), \tag{11}$$

where * denotes the complex conjugate. Assuming that the power take-off system has a linear behaviour, where the machinery force is proportional to the instantaneous position and velocity of the buoy, the load impedance may be written as:

$$\widehat{Z}_{pto}(\omega) = B_{pto}(\omega) - j\frac{K_{pto}(\omega)}{\omega}, \tag{12}$$

where K_{pto} and B_{pto} are the stiffness and damping coefficients of the PTO system respectively. Thus, substituting Equations (9) and (12) into Equation (11), optimal values of the control parameters are:

$$B_{pto}(\omega) = B(\omega), \quad K_{pto}(\omega) = \omega^2(m + A(\omega)) - C. \tag{13}$$

It can be seen from Equation (13) that for the floating WECs, the desired value of the PTO stiffness can take negative values $K_{pto}(\omega) < 0$ for the range of wave frequencies when $C > \omega^2(m + A(\omega))$. However, for the submerged buoys the PTO stiffness is always positive as $C = 0$. This is a very important feature, as the positive K_{pto} can be easily achieved by using a physical spring component, while implementation of the negative stiffness requires the reactive power flow through the PTO system which is much more difficult to achieve in practice.

3.2. Power output in irregular waves

Regular wave results presented in Section 2 demonstrate the fundamental differences between floating and submerged WECs. However, the comparison of these systems should be conducted under irregular wave time-series that more accurately represent real sea states. Assuming that the PTO system comprises spring and damping effects, the time-varying load force can be modelled similarly to Equation (12):

$$F_{pto}(t) = -B_{pto}\dot{z}(t) - K_{pto}z(t), \tag{14}$$

where $z(t)$ and $\dot{z}(t)$ are the displacement and velocity of the buoy in heave.

Depending on the control strategy, K_{pto} and B_{pto} can be tuned on a sea state basis [17] or optimised in real time on a wave by wave basis [18]. The latter strategy comes closest to the optimal reactive control in terms of the power output [19], but it requires an accurate plant model and future knowledge of the wave excitation forces. Therefore, in this work it is assumed that PTO parameters are tuned (optimised) for each sea state, which is easier to implement in practice but leads to a sub-optimal control method. Optimisation of PTO parameters is made using an exhaustive search while allowing negative values of K_{pto} for floating converters. A full description of the modelling routine and simulation set-up can be found in Appendix B.

The performance of the spherical and cylindrical WECs over the range of irregular sea states are shown in Figs. 6 and 7 respectively. The power absorption is represented in terms of the relative

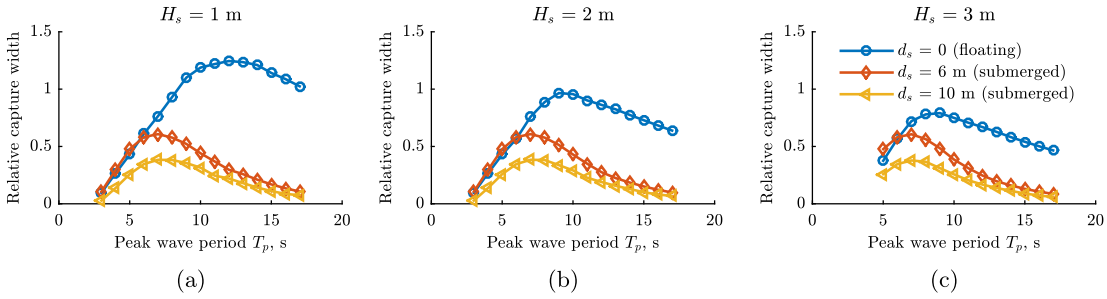

Fig. 6. Relative capture width of the floating and submerged spherical WECs in irregular waves with significant wave heights of (a) $H_s = 1$ m, (b) $H_s = 2$ m, and (c) $H_s = 3$ m over the range of peak wave periods. The sea states have been generated using a Pierson-Moskowitz wave spectrum.

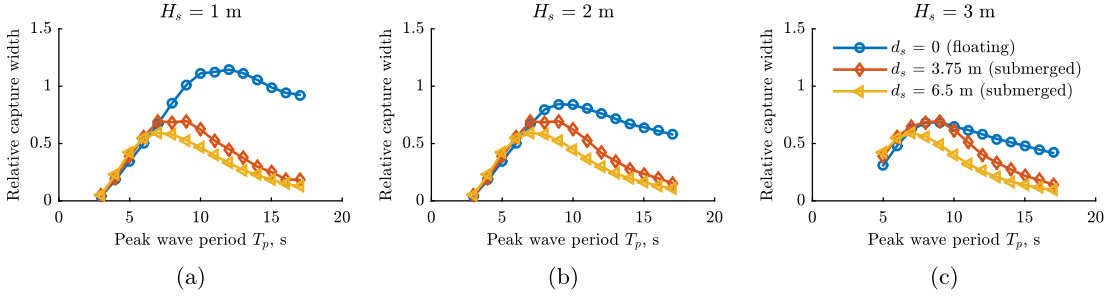

Fig. 7. Relative capture width of the floating and submerged cylindrical WECs in irregular waves with significant wave heights of (a) $H_s = 1$ m, (b) $H_s = 2$ m, and (c) $H_s = 3$ m over the range of peak wave periods. The sea states have been generated using a Pierson-Moskowitz wave spectrum.

capture width (a ratio of the absorbed power to the power that is contained in the incident wavefront of a width equal to the characteristic length of the converter). The overall trend is consistent with regular wave results: floating WECs demonstrate better performance across all sea states except several cases with $T_p < 6$ s and $H_s = 2$ and 3 m, where motion of the floating converters has already reached constraints. Also, previous findings, that the cylinder placed closer to the mean water level ($d_s = 3.75$ m) can generate more power than its floating counterpart at a range of wave periods, have not been confirmed in irregular waves.

Another interesting observation is that a sphere submerged deeper ($d_s = 10$ m) shows poorer performance across all sea states, even though according to the regular wave results all buoys should absorb the same amount of power up to wave periods of 7 s (see Fig. 3). This may be caused by the control strategy applied to all WECs which is not optimal a priori. So the performance of the system with fixed control parameters (even if they are tuned for each sea state) can be highly dependent on the WEC bandwidth.

3.3. Resonance bandwidth

Resonance (or absorption) bandwidth of the converter corresponds to the frequency range where the absorbed power stays within 50% of its maximum value. Thus, the broader the bandwidth, the less need for control. Large structures such as terminators or attenuators have broader bandwidth than point absorbers, and for the latter, increase in size leads to the bandwidth extension [20].

For comparison between floating and submerged WECs, it is necessary to understand the impact of submergence depth on the system bandwidth. Consider the response of converters when its resonance is tuned to only one wave frequency from the spectrum as in Section 3.2. Fig. 8 shows the non-dimensional power absorption of spherical bodies of $a = 5$ m radius with different submergence depths ($d_s = 0$, 6 m and 10 m) in regular waves of $H = 1$ m height with the mass of all buoys kept constant at

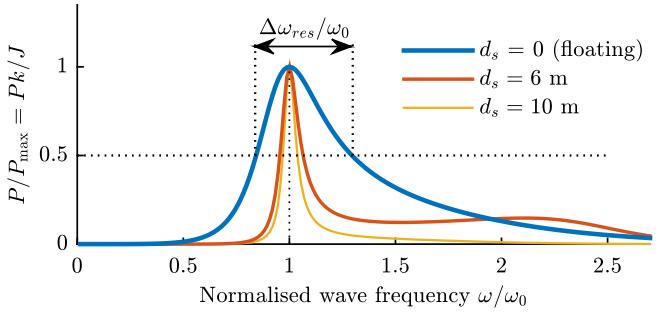

Fig. 8. Resonance bandwidth of the spherical WECs in regular waves of $H = 1$ m height: non-dimensional absorbed power vs. normalised wave frequency. Converters of 5 m radius are tuned to reach resonance at the wave frequency of $\omega_0 = 0.74$ rad/s.

$m = 0.5\rho V$. The power take-off damping and spring coefficients are chosen such that each system reaches resonance at the wave period of $T_0 = 8.5$ s ($\omega_0 = 0.74$ rad/s), allowing negative PTO stiffness for the floating case. No motion constraints are considered. The power absorption is presented as $\frac{Pk}{J}$ with a maximum possible value of 1 for the heaving body. It can be seen that the resonance bandwidth $\left(\frac{\Delta\omega_{res}}{\omega_0}\right)$ of the floating sphere is about 4 times wider than that of the submerged one. Moreover, the deeper the body is submerged, the narrower the resonance bandwidth becomes. This can be explained by the fact that the resistance (radiation damping) of the converter decreases as the immersion depth increases, which leads to a narrow bandwidth of fully submerged buoys.

Results in Fig. 8 show how the performance of the WECs deteriorates when the converter resonance is tuned to only one frequency from the spectrum. Similarly, consider a behaviour of the same converters in irregular waves when fixed controller parameters are chosen to match only one sea state from the site wave

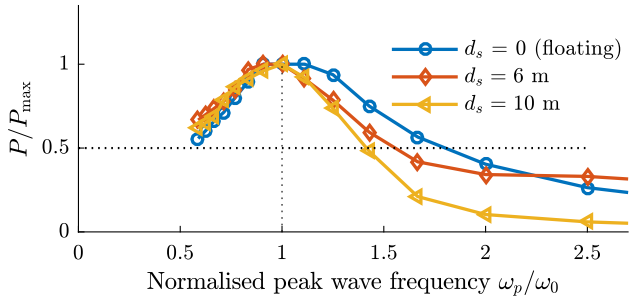

Fig. 9. Resonance bandwidth of the spherical WECs in irregular waves of $H_s = 1$ m significant wave height: non-dimensional absorbed power vs. normalised peak wave frequency. Converters of 5 m radius are tuned to the sea state with a significant wave height of $H_s = 1$ m and a peak wave period of $T_p = \frac{2\pi}{\omega_p} = 10$ s. All irregular wave time-series have been generated using a Pierson-Moskowitz wave spectrum.

climate. Thus, the non-dimensional power absorption of spherical WECs in irregular waves of $H_s = 1$ m significant wave height is shown in Fig. 9. The fixed PTO stiffness (K_{pto}) and damping (B_{pto}) coefficients are set such that each converter has maximum power output at the sea state of $H_s = 1$ m and $T_p = 10$ s. So values of P in the figure correspond to the absorbed power when one set of control gains is used across all sea states, while for $P_{\max}$ PTO parameters are optimised for each sea state. These results confirm frequency response findings: changes in the sea conditions lead to a more noticeable decrease in energy harvesting for submerged converters than for the floating one. A difference in passband width in Figs. 8 and 9 is due to the fact that bandwidth in regular waves characterises deviations from optimal control, while its value in irregular waves shows the sensitivity of the averaged absorbed power to changes in the sub-optimal controller (even with optimised parameters).

Overall, it is essential to apply optimal control to point absorbers due to their narrow bandwidth, which is even narrower for submerged cases as the bandwidth decreases with increased immersion of the buoy.

3.4. Considerations for passive phase control

Optimal control uses bi-directional power flow to manipulate the resonance frequency of the WEC, whereas there are other control strategies that can improve the power output of the system without the need for reactive power flow through the machinery. Phase control, mostly represented by latching [21,22] and declutching [23], achieves the optimal phase condition between the buoy velocity and the wave excitation force by locking or unlocking the buoy motion during parts of the oscillation cycle. Thus, latching and declutching controls refer to the 'bang-bang' strategies where the machinery force is switching between some constant and a very large value for latching and between zero and a constant value for declutching.

Latching control shows the best performance when the incident wave frequency is lower than the resonance frequency of the device ($\omega < \omega_0$) [21]. In this case, the buoy velocity leads the excitation force (see Fig. 10a) and there is only a small part of the cycle when the buoy should be kept stationary to achieve an optimal phase condition. However, when $\omega > \omega_0$, the buoy velocity lags the excitation force (see Fig. 10b) meaning that the buoy motion should be locked for at least half of the cycle which is not practical from the power absorption point of view. In contrast, the declutching control strategy performs better with systems where the natural frequency of the WEC is higher than the wave frequency ($\omega > \omega_0$) [23].

As already noted, the natural frequency of submerged converters is always lower than the incident wave frequency, whereas for the floating point absorbers its value lies at higher frequency range. Therefore, it may be concluded, that the latching control is more beneficial for the floating converter while declutching is more suitable for its submerged counterpart. However, the latter may also take advantage of the optimal latching control if to shift its resonance to the higher frequency range by an additional physical spring. These results are graphically shown on Fig. 11 along with findings on reactive control. Thus, choosing among different control strategies for submerged converters it is necessary to keep in mind their distinctive features from floating ones.

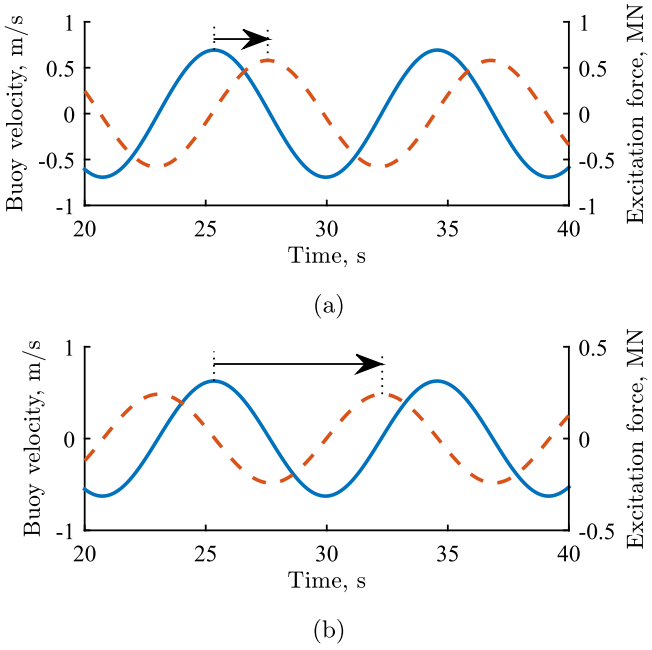

Fig. 10. Velocity (blue solid line) and excitation force (red dashed line) time series for the spherical WECs of 5 m radius under the regular wave of $H = 2$ m height and period of $T = 9$ s without any control: (a) floating and (b) submerged ($d_s = 10$ m). (For interpretation of the references to colour in this figure legend, the reader is referred to the web version of this article.)

4. Choice of a reasonable WEC size

In this section, appropriate sizes of the floating and submerged WECs are studied for several generic body shapes assuming that all buoys are optimally controlled at each wave frequency. Then, the

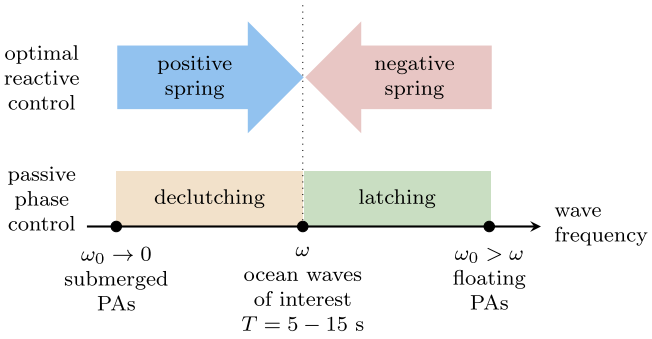

Fig. 11. The generalised diagram of the wave energy converter control depending on the location of its natural frequency with respect to the incident wave frequency.

obtained results are examined under irregular wave conditions.

According to the results presented in Section 2, floating and submerged converters should be of different sizes in order to capture the same amount of wave energy. Thus, using the upper power absorption bounds P_A and P_B, it is possible to choose an appropriate size of the WEC for a particular sea site. Falnes [1] proposed a methodology of selection of the WEC size and power take-off capacity according to the following steps:

Sea site $\rightarrow \boldsymbol{J_T}$. Choose an appropriate sea site location and determine a wave power threshold J_T (kW/m) which is being exceeded only one third of the year.

Spectrum $\rightarrow \boldsymbol{T_p}(\boldsymbol{T_e})$. Find the peak period, or the peak energy period of the most frequent waves according to the sea site probability data (T_p or T_e).

$\boldsymbol{J_T}, \boldsymbol{T_p}(\boldsymbol{T_e}) \rightarrow \boldsymbol{T}, \boldsymbol{H}$. Relate J_T and T_p to the regular wave of period $T = T_e \approx 0.858 T_p$ (for the fully developed uni-modal sea) [24] with the same wave power level. Determine the wave height of the corresponding regular wave using the equation $J_T = \frac{\rho g^2 H^2 T}{32\pi}$.

$\boldsymbol{T}, \boldsymbol{H} \rightarrow \boldsymbol{V}$. Calculate the body volume solving the equation $P_A = P_B$ that results in:

$$V = \frac{c_\infty}{c_0} H T^4. \tag{15}$$

The body chosen according to this approach will operate at full capacity for at least one third of the year.

Now consider an example assuming that there is a need to select a wave energy converter for the site where wave power level exceeds 34 kW/m about one-third of the year, a significant wave height is $H_s = 2.5–3$ m and the peak wave period is $T_p = 10$ s. This corresponds to the regular wave of $H = 2$ m and $T = 8.5$ s. Using Equation (15) it may be calculated that the volume of the floating converter regardless of shape should be 322 m^3. In the case of the submerged converters, the same methodology can be applied but using different P_B-bounds and expressing all parameters in terms of the body radius. For the submerged sphere setting the maximum displacement in heave as $s_{3,\max} = 0.67a$, the submergence depth of $d_s = 1.87a$ should ensure the operation of the body remains under water at all times. As a result, solving the equation $P_A = P_{B,s}$ (Eq. (4) = Eq. (6)) numerically with one unknown a, the size of the submerged sphere should be 696 m^3 for the same sea site, which is more than twice the required volume of the floating converter. Similarly, the volume of the cylindrical WECs should be 448 m^3 using Equations (4) and (7), and setting $h_c = a$, $d_s = 1.2a$, $s_{3,\max} = 0.5a$.

To demonstrate the effect of the body size on power efficiency, the power absorption curves for floating and submerged spherical bodies of six different radii (3–8 m) are shown on Fig. 12a and b respectively, where the displacement amplitude of all converters is constrained by $0.67a$ and the d_s distance for submerged WECs is $1.87a$. The dotted vertical line and points on curves correspond to the targeted wave period of $T = 8.5$ s.

The data on Fig. 12 can also be represented in terms of the Power-Volume correlation for the fixed wave period of interest. Thus, in order to make the analysis more generic, the spherical case shown on Fig. 12 has been complemented by three other body shapes including a cylinder, an ellipsoid (oblate spheroid) and a chamfered cylinder (see Fig. 13). Table 1 shows parameters of all systems and the correlation between them. The maximum motion of all bodies is chosen in a way that $s_{3,\max} \approx V/(2S_{xy}) = V/(2\pi a^2)$ meaning that all converters have the same volume stroke, where S_{xy} is the cross-section area of the buoy in the horizontal xy plane. The submergence depth is set such that the body of 524 m^3 volume

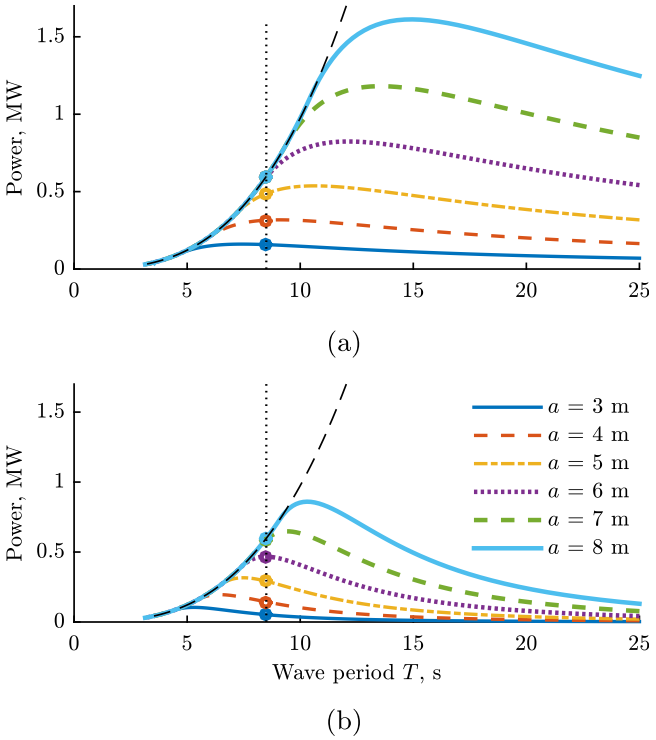

Fig. 12. Power absorbed by the (a) floating ($d_s = 0$) and (b) submerged ($d_s = 1.87a$) spherical WECs of different radii vs. wave period. Wave height is $H = 2$ m, motion of all buoys is constrained by $0.67a$. The black dashed curve corresponds to the P_A limit from Eq. (4).

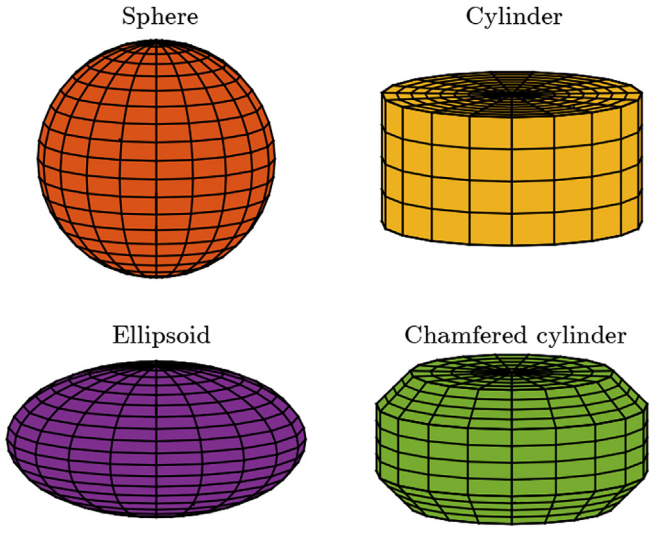

Fig. 13. Shapes of WECs used in the Power-Volume analysis.

at the maximally extended stroke has 1 m distance from its top surface to the mean water level, for other sizes this distance is scaled down or up according to the body radius. Hydrodynamic parameters of mentioned geometries have been obtained using WAMIT [12]. Mesh convergence has been checked and typical models composed of approximately 2000 panels.

The dependence of the maximum captured power on the structural volume of four bodies for the sea state of interest with $H = 2$ m, $T = 8.5$ s is demonstrated on Fig. 14. The upper limit of 0.6 MW corresponds to the maximum of P_A curve at $T = 8.5$ s, and

Table 1
Parameters of the WECs from Fig. 13.

Parameter	Notation	Sphere	Cylinder	Ellipsoid	Chamfered cylinder
Radius	a	r	$1.1r$	$r\sqrt[3]{2}\approx 1.26r$	$r\sqrt[3]{1.5}\approx 1.14r$
Height (vertical dimension)	h	$2a$	a	a	a
Volume	V	$4\pi a^3/3$	πa^3	$2\pi a^3/3$	$85\pi a^3/96$
Submergence depth	d_s	$1.87a$	$1.2a$	a	$1.1a$
Motion constraints	$s_{3,\max}$	$2a/3$	$0.5a$	$a/3$	$0.45a$

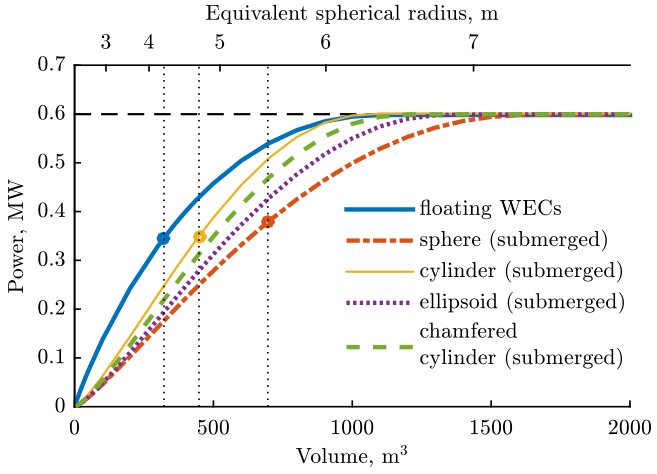

Fig. 14. Dependence of the absorbed power on the volume of WECs for the regular wave of $H = 2$ m, $T = 8.5$ s. Parameters of all buoys are taken from Table 1. The horizontal dashed line corresponds to the maximum power that can be captured from this regular wave by an oscillating axisymmetric body. Markers show optimal volumes of WECs chosen according to Falnes' methodology based on power capacity.

markers on each curve show the body volume chosen according to Falnes' methodology. Thus, the size of submerged buoys designed for the same sea site should be $1.4-2.2$ larger than the floating one with approximately the same power capacity. Interestingly, that among all submerged cases, a body with a cylindrical shape should be the smallest while the spherical buoy should be the largest to generate the same amount of power. The desired volumes of the ellipsoid and chamfered cylinder are estimated to be somewhere in-between.

In addition to the absolute values of power and volume, the power-to-volume ratio is also of interest as it can be indirectly related to the estimation of the converter cost [25]. It has been observed that for the heaving point absorbers the smaller the physical volume of the body, the larger the power-to-volume ratio [26]. To demonstrate the impact of this relationship, it has been calculated for five different systems based on the information from Fig. 14. Power has been normalised according to the Froude scaling law choosing the wavelength $\lambda = 2\pi/k = g/(2\pi)T^2$ as a length parameter:

$$P_n = \frac{P}{\lambda^{3.5}}, V_n = \frac{V}{\lambda^3}, \tag{16}$$

and is presented in Fig. 15. Thus, for the floating converters the power-to-volume ratio decreases with an increase in WEC volume. However, for submerged bodies there is a range of volumes where this ratio takes the maximum value which shows the importance of proper selection of the buoy size. Therefore, based on the maximum value of the power-to-volume ratio, the size of the submerged cylinder should be approximately 420 m^3, which is very close to 448 m^3 found using Falnes' methodology.

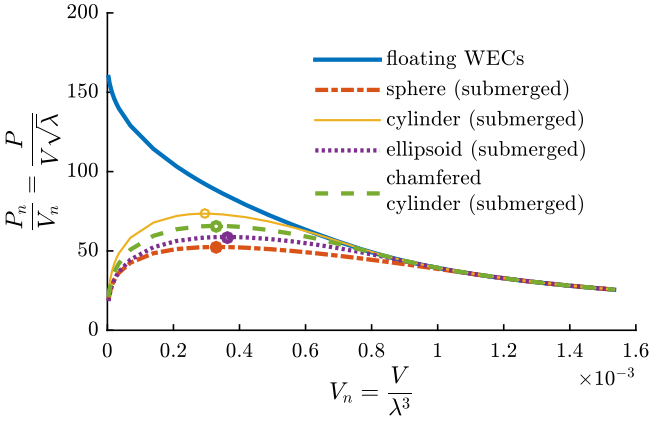

Fig. 15. Power-to-volume ratios vs. buoy volume normalised to the wavelength for floating and submerged WECs.

In order to investigate whether converters of the volumes found above have similar power absorption potential, their performance is investigated in the sea state with a significant wave height $H_s = H\sqrt{2} = 2.83$ m and a peak wave period $T_p = T_e/0.858 = 10$ s. Thus, the following buoy geometries are included in the irregular wave analysis: a floating cylinder of 322 m^3, a submerged sphere of 696 m^3, a submerged cylinder of 448 m^3, a submerged ellipsoid of 600 m^3 and a submerged chamfered cylinder of 510 m^3. All other geometric parameters can be calculated using Table 1. It is assumed that control gains are optimised on the sea state basis (see Equation (14)) which are optimised to provide maximum power. As a result, an averaged absorbed power and a relative capture width are presented in Fig. 16. Colour bars on the left show the averaged absorbed power, while dark blue bars on the right correspond to

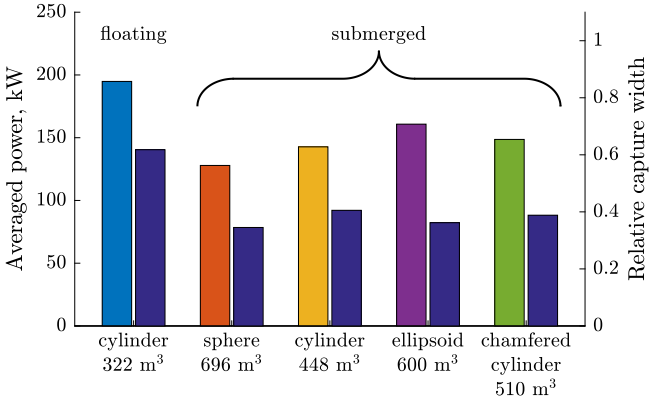

Fig. 16. Levels of the averaged absorbed power (colour bars on the left) and relative capture width (dark blue bars on the right) of the floating and submerged converters at the irregular wave time-series of $H_s = 2.83$ m and $T_p = 10$ s. Parameters of all buoys are taken from Table 1. (For interpretation of the references to colour in this figure legend, the reader is referred to the web version of this article.)

the relative capture width of each converter.

Despite the fact that all converters have been designed for this particular sea site, they demonstrate power production levels lower than expected from the regular wave analysis. This is due to sub-optimal control applied to all cases, which once again demonstrates the importance of the control strategy for the WEC development. In addition, although all submerged converters have lager volumes than their floating counterpart, their power absorption is still around 1.2–1.5 times lower than that of the floating cylinder. This means that fully submerged buoys should be even larger than shown in Fig. 14 in order to match the total power of the floating converter.

Overall, for the same power output submerged WECs should be at least 1.5 times larger than their floating counterparts where the exact volume ratio is the subject to control, shape, submergence depth and other parameters.

5. Array of small WECs vs. a large buoy of equal volume

According to the findings presented in Section 4, in particular Fig. 15, floating wave energy converters of small size are more beneficial when employed for wave power generation in comparison with large ones in terms of the power-to-volume ratio. According to Budal's diagram (as cited in Ref. [1]), the volume in Equation (5) does not necessary represent the size of one unit, and it can be interpreted as a total volume of all converters within the wave energy array. It has been shown that a compact array of small buoys can capture much more power than a single WEC of equal volume, with the advantage of having wider bandwidth [27], however, this comparison was based on the floating truncated cylinders that are tuned to their natural frequency of oscillation, not optimally controlled.

A similar analysis for the fully submerged converters is performed here but applying optimal control across the entire range of wave periods. One relatively large spherical buoy of $a = 5$ m radius has a displaced volume of $V = 524$ m^3. This volume alternatively can be formed using an array of smaller converters, e.g. 5 units of 3m-buoys, 125 units of 1m-buoys or 1000 units of 0.5m-buoys. Of course, the same volume does not guarantee the same manufacturing cost given the different surface areas, but production of buoys in large quantities will inevitably lead to lower unit manufacturing costs.

The amount of power extracted by each array in regular waves of 2 m height is presented in Fig. 17 for the floating ($d_s = 0$) and fully submerged ($d_s = 1.87a$) cases of WECs, where all spheres have a maximum stroke of $0.67a$. The energy absorbed by each array has been calculated by multiplying the power from an individual WEC by the number of units within the array but neglecting to take into account possible hydrodynamic interaction between buoys. As a result, in the case of floating systems, smaller units have higher power absorption than a single large buoy across the entire range of wave periods.

This conclusion, however, is not applicable to the fully submerged WECs as the performance of the array drops dramatically with a decrease of the buoy size at long wavelengths. It seems that the “small is beautiful” adage of Falnes [1] only applies to floating WECs, not submerged. As a result, for sites with low frequency waves using submerged converters it would be more beneficial to design one large buoy that will have the best performance at the targeted sea site than to consider smaller units of equal volume.

WECs chosen according to Falnes' methodology are designed for one dominant wave of the particular sea site. However, due to the irregular nature of ocean waves and due to the fact that submerged converters are effective power absorbers only within a specific

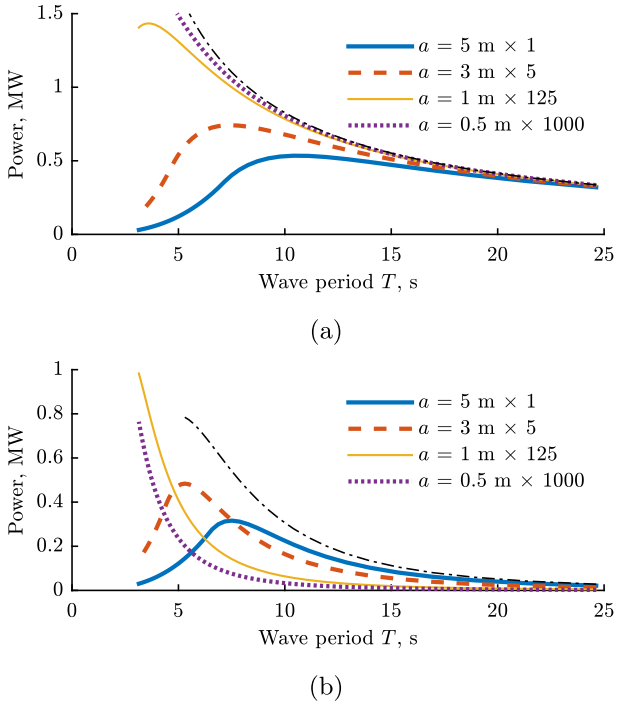

Fig. 17. Power absorbed by (a) floating ($d_s = 0$) and (b) submerged ($d_s = 1.87a$) wave arrays of the same total volume $V \approx 524$ m^3 in regular waves of 2 m height. The radius and number of units within the array is specified in the legend. Dash-dotted curves correspond to the P_B limit of the 5m-buoy. The displacement in heave of all converters is constrained by $0.67a$.

range of wave periods, it could be advantageous to form an array from the buoys of several different sizes, similar to [28,29]. Thereby each converter will target a particular wave frequency from the spectrum while maximising the power absorption of the entire farm.

6. Combination of modes

The combination of motion modes in wave power absorption is attractive due to increased efficiency and bandwidth. For example, Salter's duck [2] utilises surge, heave and pitch oscillations in order to capture the maximum power available in the wave. Another solution has been offered in Refs. [30–32] introducing three cables connected to the spherical buoy in order to make the surge mode controllable by the power take-off system. Therefore, the power efficiency of submerged and floating WECs with different motion modes is compared in this section.

Surging and heaving floating converters radiate different types of waves that lead to different power absorption. According to Equation (1) the P_A-bound of the surging body is twice as high as that of the converter that moves in heave only [5]. The low frequency limits P_B are also different for these motion modes where Equation (6) describes heave oscillation, while an expression for the surging floating sphere has a form of [10]:

$$P_{B,f}^{surge} = 2\pi^3 \rho s_{1,\max} \frac{VH}{T^3}. \tag{17}$$

Analysing Equations (5) and (17), it is clear, that the P_B-bound for the surging body is $\mathcal{O}(T^{-3})$, while for the heaving body this bound has a smaller decay rate and is $\mathcal{O}(T^{-1})$. These results are very similar to the previous comparison of floating and submerged heaving bodies meaning that the surging floating sphere is a poorer

power absorber at long wavelengths than the same body that oscillates in heave. Comparing motion modes of the floating sphere the following features should be outlined:

$$-P_A^{surge} = 2P_A^{heave};$$

$$-P_{B,f}^{surge} = \mathscr{O}\left(T^{-3}\right), \text{ while } P_{B,f}^{heave} = \mathscr{O}\left(T^{-1}\right).$$

Unlike floating converters, fully submerged buoys have almost the same power efficiency from oscillations in heave or surge. Thus, the P_B-bounds for the surging and heaving submerged spheres have the same expressions described by Equation (6) which has been shown in Ref. [10]. Hence, for the fully submerged spherical WEC:

$$-P_A^{surge} = 2P_A^{heave},$$

$$-P_{B,s}^{surge} = P_{B,s}^{heave} = \mathscr{O}\left(T^{-3}\right).$$

The difference in power efficiency between surging and heaving spheres is demonstrated in Fig. 18. The sphere radius is $a = 5$ m, motion in surge (mode 1) and heave (mode 3) is constrained by $s_{1,\max} = s_{3,\max} = 0.67a = 3.3$ m, submergence depths are $d_s = 0$ m, $1.2a = 6$ m and $2a = 10$ m, wave height is taken as $H = 2$ m. It can be seen, that at longer wave periods heave motion is dominant for floating converters showing that the power contribution from the surge mode may be marginal for floating systems. In contrast, a submerged sphere that oscillates in surge is more efficient across the entire frequency range. Therefore, the power efficiency of the submerged system may increase by two to three times due to the additional controllable degree of freedom. Also, the ratio between power levels from surge and heave does not change with a submergence depth as shown in Fig. 18b and c. It should be noted that the surging floating sphere utilises only half of its volume to couple with the fluid (at nominal depth), while for a submerged sphere the total volume is involved in power absorption. This explains why the power level of a surging floating sphere is lower than that of a fully submerged one.

For comparison, similar plots are presented for the vertical cylinder of $h_c = a = 5.5$ m on Fig. 19. Motion constraints in each mode are calculated as $s_{1,\max} = V/(2S_{xz}) = \pi a^2 h_c/(4ah_c) = \pi a/4 = 4.32$ m and $s_{3,\max} = V/(2S_{xy}) = \pi a^2 h_c/(2\pi a^2) = a/2 = 2.75$ m in order to have equal volume stroke [10] in surge and heave. Interestingly, that for the vertical cylinder placed closer to the water surface ($d_s = 3.75$ m) at higher wave frequencies surge is dominant, while for low-frequency waves more power can be absorbed from heave. When the cylinder is submerged deeper ($d_s = 6.5$ m), the situation is closer to the spherical case, where the surging body captures more power across entire range of wave periods. As a result, the power distribution between motion modes for the fully submerged bodies depends on the submergence depth and the aspect ratio of the converter and a clear trend cannot be identified, as in the case of floating systems.

Based on this analysis, it may be concluded that employment of several motion modes in power generation is more advantageous for the fully submerged converters, while such a benefit for the floating counterparts will be marginal.

7. Conclusion

The comparison between floating and fully submerged WECs has been performed in order to identify main distinctive features between the systems. The analysis has been carried out in regular

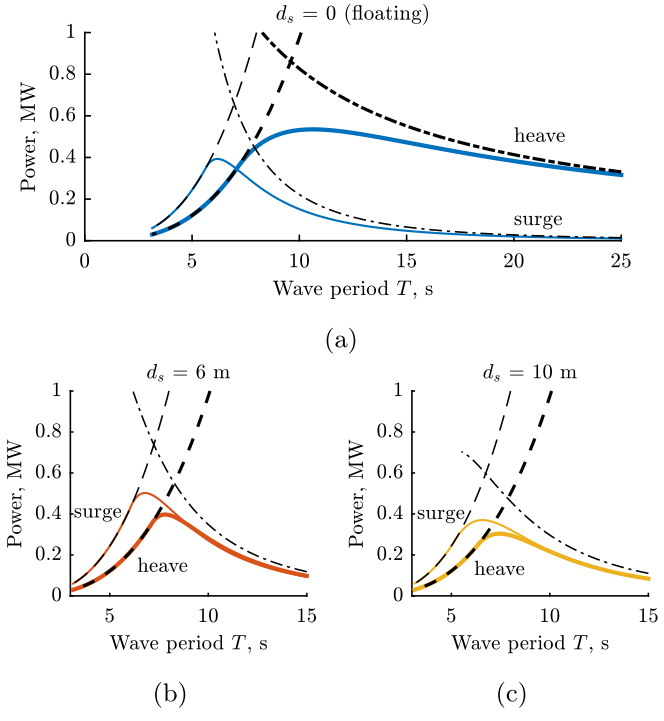

Fig. 18. The power absorbed by the surging and heaving spherical WECs of 5 m radius with different submergence depth: (a) floating $d_s = 0$ and submerged (b) $d_s = 6$ m, (c) $d_s = 10$ m. Motion amplitudes in heave and surge are constrained by $s_{1,\max} = s_{3,\max} = 0.67a = 3.3$ m. Wave height is set to $H = 2$ m. The dashed curves correspond to the P_A limit from Eq. (4), and dash-dotted curves show the P_B bounds from Eqs. (5) and (6).

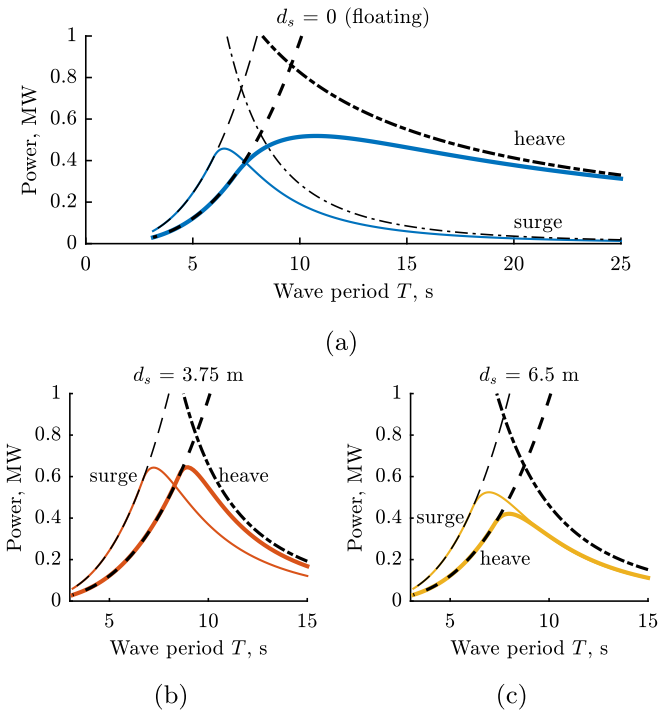

Fig. 19. The power absorbed by the surging and heaving vertical cylinders ($h_c = a = 5.5$ m) with different submergence depth: (a) floating $d_s = 0$ and submerged (b) $d_s = 3.75$ m, (c) $d_s = 6.5$ m. Displacements in surge and heave are constrained by $s_{1,\max} = \pi a/4 = 4.32$ m and $s_{3,\max} = a/2 = 2.75$ m respectively. Regular wave height is set to $H = 2$ m.

and irregular waves using a linear wave theory approximation for axisymmetric point absorbers that extract wave energy from heave or surge motion, or both.

Examples of two generic shapes (sphere and vertical cylinder) have shown that the efficiency of submerged converters is poorer than that of the floating ones at long wavelengths, while there is a narrow range of wave periods where the performance of submerged cylindrical buoys could be superior than that of its floating counterpart. In addition, WEC bandwidth decreases as the submergence depth of the buoy increases indicating the need for reactive control for the fully submerged converters. The absence of the hydrostatic restoring force for the submerged buoys affects the implementation of control strategies for this converter type. Thus, floating converters may benefit from latching phase control, whereas declutching is more suitable for submerged systems. To achieve the same level of generated power, buoys placed under water should be 1.4–2.2 times larger than those that operate on the water surface. Thus, the size of the fully submerged WECs should be chosen according to the targeted wave climate and cannot be replaced by the array of smaller converters of equal volume. Finally, submerged buoys would benefit more from multiple degrees of freedom than their floating counterparts.

The above analysis may give the impression than submerged buoys are less favourable energy converters. It should be noted, that the main objective of this study is not to show which WEC is better, but to clarify some differences in performance and design criteria. While the current paper is restricted to axisymmetric buoy shapes, there are some examples when submerged converters demonstrated good power absorption abilities. Thus, several solutions of maximising energy harvesting of submerged WECs have been offered so far: (i) to use a device with a dynamically changing volume (e.g. Archimedes Wave Swing device [33]); (ii) to keep the body submerged as close as possible to the mean water level (e.g. CETO system [34]); or (iii) to use a terminator body which inherently has a broad resonance bandwidth (e.g. the Bristol cylinder [35,36]). In addition, as previously mentioned, submerged converters have a number of advantages which may be essential from the economic perceptive.

Appendix A. Estimation of the upper bound of the absorbed power for the submerged cylinder that oscillates in heave

The average power absorbed by the oscillating body can be calculated as [5]:

$$P = \frac{1}{2}\left|\widehat{F}_{exc}\right|\left|\widehat{u}\right|\cos\phi - \frac{1}{2}B\left|\widehat{u}\right|^2 \le \frac{1}{2}\left|\widehat{F}_{exc}\right|\left|\widehat{u}\right|, \tag{A.1}$$

where $\widehat{F}_{exc}$ is the excitation force amplitude, $\widehat{u}$ is the amplitude of the body velocity, ϕ is the phase angle between the excitation force and the buoy velocity and B is the hydrodynamic damping coefficient.

The excitation force exerted on the body in the j-direction is:

$$\widehat{F}_{exc,j} = -\iint_S \widehat{p}(x,y,z)n_j\, dS, \tag{A.2}$$

where $\widehat{p}(x,y,z)$ is the complex amplitude of the hydrodynamic pressure on the body surface, n_j is the unit normal to the body surface pointing inside the water domain and dS is the surface element of wet surface S.

Hals [10] showed, that the hydrodynamic pressure $\widehat{p}$ on the body surface will never be larger than $\sigma\widehat{p}_0$, where $\sigma = 2$, $\widehat{p}_0 = p_0 e^{i(-kx+\phi_\zeta)}e^{kz}$ is the pressure amplitude of the undisturbed incident wave, $p_0 = \rho g\zeta_0 = \rho gA$ and ϕ_ζ is the phase angle of the incident wave. As a result:

$$\widehat{p}(x,y,z) \le \sigma\widehat{p}_0 = \sigma\rho gAe^{i(-kx+\phi_\zeta)}e^{kz}. \tag{A.3}$$

In order to derive the simplified equation of the heave excitation force for the submerged cylinder, cylindrical coordinates (r,θ,z) are introduced leading to $dS = r\,dr\,d\theta$, where $0 \le r \le a$ and $0 \le \theta \le 2\pi$. Also, pressure in Equation (A.2) should be integrated over two surface areas: top $(\widehat{p}_t)$ and bottom $(\widehat{p}_b)$ faces of the truncated cylinder. Thus,

$$\widehat{F}_{exc,3} = \int_0^a\int_0^{2\pi}(\widehat{p}_t(r,\theta,-d_1) - \widehat{p}_b(r,\theta,-d_2))r\,dr\,d\theta. \tag{A.4}$$

The hydrodynamic pressure on the cylinder bottom can be described by Equation (A.3):

$$\widehat{p}_b(r,\theta,-d_2) \le \sigma\rho gAe^{i(-kr\cos\theta+\phi_\zeta)}e^{-kd_2}. \tag{A.5}$$

However, for the cylinder top free-surface effects are more significant due to the possible resonance amplification of waves in the water domain above the cylinder and, therefore, the hydrodynamic pressure cannot be simplified using e^{kz} function. Thus, taking the first order approximation for the upper domain from Ref. [37], the hydrodynamic pressure on the cylinder top can be expressed as:

$$\widehat{p}_t(r,\theta,-d_1) \approx \rho gAe^{i(-kr\cos\theta+\phi_\zeta)}\frac{J_0(\kappa r)}{J_0(\kappa a)\cosh\kappa d_1}, \tag{A.6}$$

where J_0 and J_1 are Bessel functions of the first kind of order 0 and 1 respectively, κ is the real solution of the dispersion equation $\omega^2 = g\kappa\tanh(\kappa d_1)$, which can be approximated by $\omega^2 = \kappa^2 g d_1$ using shallow water conditions for the water domain above the cylinder.

Inserting Equations (A.5)–(A.6) into (A.4) and using $e^{-ikr\cos\theta} = \cos(-kr\cos\theta) + i\sin(-kr\cos\theta)$, $|\sin(-kr\cos\theta)| \le |kr\cos\theta|$, $|\cos(-kr\cos\theta)| < 1$, the approximate expression of the excitation force is:

$$\begin{aligned}\left|\widehat{F}_{exc,3}\right| &\le \left|\sigma\rho gA\int_0^a\int_0^{2\pi}\left(\frac{J_0(\kappa r)}{J_0(\kappa a)\cosh\kappa d_1} - e^{-kd_2}\right)r\,dr\,d\theta\right| \\ &= \left|\sigma\rho gA\pi\left(\frac{2aJ_1(\kappa a)}{\kappa J_0(\kappa a)\cosh(\kappa d_1)} - a^2e^{-kd_2}\right)\right|.\end{aligned} \tag{A.7}$$

For the deeper submerged bodies and if $\kappa a \to 0$, then $J_0(\kappa a) \to 1$ and $J_1(\kappa a) \to \frac{\kappa a}{2}$ and Equation (A.7) can be further simplified to:

$$\left|\widehat{F}_{exc,3}\right| \le \left|\sigma\rho gA\pi a^2\left(\frac{1}{\cosh(\kappa d_1)} - e^{-kd_2}\right)\right|. \tag{A.8}$$

Finally, given the expression for the excitation force and setting $|\widehat{u}_3| \le \omega s_{3,\max}$, the upper power bound for the heaving submerged cylinder is:

$$\begin{aligned}P &\le \frac{1}{2}\left|\widehat{F}_{exc,3}\right|\left|\widehat{u}_3\right| \\ &\le \left|\sigma\rho gA\pi\left(\frac{2aJ_1(\kappa a)}{\kappa J_0(\kappa a)\cosh(\kappa d_1)} - a^2e^{-kd_2}\right)\right|\left|\widehat{u}_3\right| \\ &= \frac{\pi^2 a\rho gH}{T}s_{3,\max}\left(\frac{2J_1(\kappa a)}{\kappa J_0(\kappa a)\cosh(\kappa d_1)} - ae^{-kd_2}\right).\end{aligned} \tag{A.9}$$

Appendix B. Time-domain model of the wave energy converter

The most common mathematical model that describes a time-domain response of the wave energy converter in waves is the Cummins equation [38]:

$$(m + A_\infty)\ddot{z} + \int_0^t K_{rad}(t-\tau)\dot{z}(\tau)d\tau + Cz = F_{exc} + F_{pto} + F_{hs}, \tag{B.1}$$

where m is a buoy mass, A_∞ is the infinite-frequency added mass coefficient, C is the hydrostatic stiffness, $K_{rad}(t)$ is the radiation impulse response function, F_{exc} is the wave excitation force, F_{pto} is the load force exerted on the buoy from the power take-off system, and F_{hs} is the additional force that keeps the body motion within allowed boundaries similar to the physical hard stop mechanism.

The load force is modelled as a linear spring-damper system:

$$F_{pto} = -B_{pto}\dot{z} - K_{pto}z, \tag{B.2}$$

where K_{pto} and B_{pto} are the PTO stiffness and damping coefficients (control parameters). To constrain the motion of the buoy, the hard stop system is modelled by a repulsive energy potential [39]:

$$\begin{aligned} F_{hs} = &-K_{hs,\min}(z - z_{\min})u(z_{\min} - z) \\ &-K_{hs,\max}(z - z_{\max})u(z - z_{\max}), \end{aligned} \tag{B.3}$$

where $u(\cdot)$ is Heaviside step function, $K_{hs,\min}$ and $K_{hs,\max}$ are the hard stop spring coefficients, $z_{\min}$ and $z_{\max}$ are the stroke limits relative to the nominal position of the converter. The effect of this force is not taken into account while calculating useful absorbed energy.

Equation (B.1) has been implemented in Simulink/MATLAB [40] with a time step of 0.01 s using the ode23s solver. The duration of all simulation runs has been set to $300 \times T_p$ but not less than 1200 s and the first $15 \times T_p$ have not been included in the analysis due to the initial transient state. Hydrodynamic (excitation and radiation) forces have been calculated using WAMIT [12]. The convolution integral in Equation (B.1) has been replaced by the state-space model using the Marine System Simulator toolbox [41]. The irregular wave time-series have been implemented using the Pierson-Moskowitz wave spectrum [24].

The mass of all floating and submerged buoys is kept as $m = 0.5\rho V$. Values of motion constraints are specified in Table 1 for each buoy geometry under consideration. The hard stop spring coefficient is set to $K_{hs,\min} = K_{hs,\max} = 10^8$N/m. Unless otherwise stated, the PTO control parameters K_{pto}, B_{pto} are optimised for each sea state using brute-force search.

References

[1] J. Falnes, J. Hals, Heaving buoys, point absorbers and arrays, Philos. Trans. R. Soc. A Math. Phys. Eng. Sci. 370 (1959) (2012) 246–277.
[2] S.H. Salter, World progress in wave energy − 1988, Int. J. Ambient Energy 10 (1) (1989) 3–24.
[3] K. Budal, J. Falnes, A resonant point absorber of ocean-wave power, Nature 256 (5517) (1975) 478–479.
[4] D.V. Evans, A theory for wave-power absorption by oscillating bodies, J. Fluid Mech. 77 (1) (1976) 1–25.
[5] J. Falnes, Ocean Waves and Oscillating Systems: Linear Interactions Including Wave-energy Extraction, Cambridge University Press, 2002.
[6] J. Cruz, Ocean Wave Energy: Current Status and Future Perspectives, Green Energy and Technology, Springer Berlin Heidelberg, Berlin, 2008.
[7] D.V. Evans, Maximum wave-power absorption under motion constraints, Appl. Ocean Res. 3 (4) (1981) 200–203, http://dx.doi.org/10.1016/0141-1187(81)90063-8.
[8] D.J. Pizer, Maximum wave-power absorption of point absorbers under motion constraints, Appl. Ocean Res. 15 (4) (1993) 227–234, http://dx.doi.org/10.1016/0141-1187(93)90011-L.
[9] K. Budal, J. Falnes, Interacting point absorbers with controlled motion, in: B. Count (Ed.), Power from Sea Waves, UK, Academic Press, London, 1980, pp. 381–399.
[10] J.H. Todalshaug, Practical limits to the power that can be captured from ocean waves by oscillating bodies, Int. J. Mar. Energy 3–4 (2013) e70–e81.
[11] J. N. Newman, The interaction of stationary vessels with regular waves, Proceedings of the 11th Symposium on Naval Hydrodynamics, 491, 501.
[12] C.-H. Lee, Wamit Theory Manual, 1995.
[13] S. Chakrabarti, Handbook of Offshore Engineering (2-volume Set), Elsevier, 2005.
[14] J.W. Miles, Resonant amplification of gravity waves over a circular sill, J. Fluid Mech. 167 (1986) 169–179.
[15] P. McIver, D. Evans, The occurrence of negative added mass in free-surface problems involving submerged oscillating bodies, J. Eng. Math. 18 (1) (1984) 7–22.
[16] J.V. Ringwood, G. Bacelli, F. Fusco, Energy-maximizing control of wave-energy converters: the development of control system technology to optimize their operation, Control Syst. IEEE 34 (5) (2014) 30–55, http://dx.doi.org/10.1109/MCS.2014.2333253.
[17] B. Ding, B.S. Cazzolato, M. Arjomandi, P. Hardy, B. Mills, Sea-state based maximum power point tracking damping control of a fully submerged oscillating buoy, Ocean Eng. 126 (2016) 299–312.
[18] J. Hals, J. Falnes, T. Moan, A comparison of selected strategies for adaptive control of wave energy converters, J. Offshore Mech. Arct. Eng. 133 (3) (2011), 031101–031101.
[19] J. Hals, J. Falnes, T. Moan, Constrained optimal control of a heaving buoy wave-energy converter, J. Offshore Mech. Arct. Eng. 133 (1) (2011) 011401.
[20] M. Folley, Numerical Modelling of Wave Energy Converters: State-of-the-art Techniques for Single Devices and Arrays, Saint Louis, Elsevier Science, Saint Louis, 2016.
[21] A. Babarit, A.H. Clément, Optimal latching control of a wave energy device in regular and irregular waves, Appl. Ocean Res. 28 (2) (2006) 77–91, http://dx.doi.org/10.1016/j.apor.2006.05.002.
[22] P. Hardy, B.S. Cazzolato, B. Ding, Z. Prime, A maximum capture width tracking controller for ocean wave energy converters in irregular waves, Ocean Eng. 121 (2016) 516–529, http://dx.doi.org/10.1016/j.oceaneng.2016.05.045.
[23] A. Babarit, M. Guglielmi, A.H. Clément, Declutching control of a wave energy converter, Ocean Eng. 36 (1213) (2009) 1015–1024, http://dx.doi.org/10.1016/j.oceaneng.2009.05.006.
[24] The Specialist Committee on Waves, Final report and recommendations to the 23rd ITTC, in: Proceedings of the 23rd International Towing Tank Conference, vol. II, pp. 505–736.
[25] A. Babarit, J. Hals, M. Muliawan, A. Kurniawan, T. Moan, J. Krokstad, Numerical benchmarking study of a selection of wave energy converters, Renew. Energy 41 (2012) 44–63.
[26] J. Falnes, Optimum control of oscillation of wave-energy converters, Int. J. Offshore Polar Eng., 12, 02.
[27] X. Garnaud, C. Mei, Comparison of wave power extraction by a compact array of small buoys and by a large buoy, IET Renew. Power Gener. 4 (6) (2010) 519–530.
[28] M. Göteman, J. Engström, M. Eriksson, J. Isberg, M. Leijon, Methods of reducing power fluctuations in wave energy parks, J. Renew. Sustain. Energy 6 (4) (2014) 043103.
[29] J. Wu, S. Shekh, N. Sergiienko, B. Cazzolato, B. Ding, F. Neumann, M. Wagner, Fast and effective optimisation of arrays of submerged wave energy converters, in: Proceedings on Genetic and Evolutionary Computation Conference (GECCO-2016), 2016.
[30] M.A. Srokosz, The submerged sphere as an absorber of wave power, J. Fluid Mech. 95 (4) (1979) 717–741.
[31] J.T. Scruggs, S.M. Lattanzio, A.A. Taflanidis, I.L. Cassidy, Optimal causal control of a wave energy converter in a random sea, Appl. Ocean Res. 42 (2013) 1–15, http://dx.doi.org/10.1016/j.apor.2013.03.004.
[32] N.Y. Sergiienko, B.S. Cazzolato, B. Ding, M. Arjomandi, An optimal arrangement of mooring lines for the three-tether submerged point-absorbing wave energy converter, Renew. Energy 93 (2016) 27–37, http://dx.doi.org/10.1016/j.renene.2016.02.048.
[33] D. Valério, P. Beirão, J. Sá da Costa, Optimisation of wave energy extraction with the Archimedes wave swing, Ocean Eng. 34 (1718) (2007) 2330–2344, http://dx.doi.org/10.1016/j.oceaneng.2007.05.009.
[34] Carnegie Wave Energy Limited, What is CETO?, accessed 15 January 2015 (n.d.). URL http://www.carnegiewave.com/ceto-technology/what-is-ceto.html.
[35] D.V. Evans, D.C. Jeffrey, S.H. Salter, J.R.M. Taylor, Submerged cylinder wave energy device: theory and experiment, Appl. Ocean Res. 1 (1) (1979) 3–12, http://dx.doi.org/10.1016/0141-1187(79)90003-8.
[36] S.H. Crowley, R. Porter, D.V. Evans, A submerged cylinder wave energy converter with internal sloshing power take off, Eur. J. Mech. - B/Fluids 47 (2014) 108–123, http://dx.doi.org/10.1016/j.euromechflu.2014.03.008.

[37] S. Jiang, Y. Gou, B. Teng, D. Ning, Analytical solution of a wave diffraction problem on a submerged cylinder, J. Eng. Mech. 140 (1) (2014) 225–232, http://dx.doi.org/10.1061/(ASCE)EM.1943-7889.0000637.
[38] W.E. Cummins, The Impulse Response Function and Ship Motions, Report, DTIC Document, 1962.
[39] A. Babarit, J. Hals, M. Muliawan, A. Kurniawan, T. Moan, J. Krokstad, Numerical Estimation of Energy Delivery from a Selection of Wave Energy Converters – Final Report, Report, Ecole Centrale de Nantes & Norges Teknisk-Naturvitenskapelige Universitet, 2011.
[40] The Mathworks Inc., MATLAB, version 8.5.0.197613 (R2015a) (2015).
[41] T. Perez, T.I. Fossen, A MATLAB toolbox for parametric identification of radiation-force models of ships and offshore structures, Model. Identif. Control 30 (1) (2009) 1.